Fennel Katja (Orcid ID: 0000-0003-3170-2331)
Laurent Arnaud (Orcid ID: 0000-0002-8545-9309)

Quantifying the relative importance of riverine and open-ocean nitrogen sources for hypoxia formation in the northern Gulf of Mexico

Fabian Große[1], Katja Fennel[1], and Arnaud Laurent[1]

[1] Department of Oceanography, Dalhousie University, Halifax, NS, Canada

Corresponding author: Fabian Große (fabian.grosse@dal.ca)

Key Points:

- Relative contributions of different nitrogen sources to hypoxia formation in the northern Gulf of Mexico during 2001-2011 are quantified
- Mississippi (51±9%) and Atchafalaya River nitrogen (33±9%) supports most of sediment oxygen consumption, the main oxygen sink on the shelf
- A combined nitrogen load reduction and discharge diversion towards the Atchafalaya River does not appear viable for hypoxia mitigation

This article has been accepted for publication and undergone full peer review but has not been through the copyediting, typesetting, pagination and proofreading process which may lead to differences between this version and the Version of Record. Please cite this article as doi: 10.1029/2019JC015230

Abstract

The Mississippi and Atchafalaya River System discharges large amounts of freshwater and nutrients into the northern Gulf of Mexico (NGoM). These lead to increased stratification and elevate primary production (PP) in the outflow region. Consequently, hypoxia (oxygen < 62.5 mmol m^{-3}), extending over an area of roughly 15,000 km^2, forms every summer in bottom waters. High-resolution models have significantly improved our understanding of the processes controlling hypoxia formation in the NGoM and have strongly implicated riverine nutrients as the dominant nutrient source. However, the relative importance of different nutrient sources (i.e. the Mississippi and Atchafalaya Rivers and offshore) has not been assessed before now. Here, we combine a high-resolution model with an element tracing method to directly quantify the relative contributions of nitrogen from the two rivers and the open ocean to PP and sediment oxygen consumption (SOC), which is the main oxygen sink contributing to hypoxia in the NGoM. Our results indicate that, averaged over 2001–2011, Mississippi and Atchafalaya nitrogen support 51±9% and 33±9% of summer SOC, respectively, while open-ocean nitrogen supports 16±2%. The higher relative impact of Mississippi inputs results from longer transit times compared to those of Atchafalaya inputs. We also analyze the effect of riverine nitrogen load reductions and a larger diversion of discharge to the Atchafalaya River. These scenario simulations show that nutrient load reductions are most effective in mitigating hypoxia.

Plain Language Summary

The availability of oxygen in marine waters is crucial for many marine animals. In the northern Gulf of Mexico a large area of low-oxygen conditions forms every summer due to large nutrient and freshwater inputs from the Mississippi and Atchafalaya Rivers, which stimulate algal growth. The algae eventually sink and decompose near the sea floor using the oxygen available in subsurface waters.

Computer-based models that simulate the interactions between circulation and biological processes are important tools to better understand the mechanisms leading to low-oxygen conditions. Here, we combine such model with a method that allows us to quantify the relative contributions of nitrogen from the Mississippi and Atchafalaya Rivers and the open ocean to the formation of low-oxygen conditions in the northern Gulf of Mexico.

Our results suggest that Mississippi and Atchafalaya nitrogen are responsible for about a half and a third of the oxygen consumption leading to low-oxygen conditions, respectively, while open ocean nitrogen contributes less than 20%.

1 Introduction

Availability of dissolved oxygen (O_2) is essential for most multicellular marine organisms (e.g. Díaz & Rosenberg, 1995; Rosenberg et al., 1991). A shortage of O_2, referred to as hypoxia (O_2 < 62.5 mmol O_2 m^{-3}), can have severe impacts on marine biodiversity and ecosystem functioning (Gray et al., 2002; Levin et al., 2009; Vaquer-Sunyer & Duarte, 2008). In coastal seas, hypoxia formation primarily depends on the balance between O_2 supply from photosynthesis and exchange with the atmosphere, and O_2 consumption due to degradation of organic matter (Díaz & Rosenberg, 2008), although lateral supply of oxygen-rich or oxygen-poor water can play an important role as well (Fennel & Testa, 2019). Coastal hypoxia is reported to have increased exponentially since the middle of the 20th century, primarily due to increased anthropogenic nutrient inputs from land, which stimulate organic matter production (Breitburg et al., 2018; Díaz & Rosenberg, 2008)

The northern Gulf of Mexico (NGoM) receives large amounts of freshwater (FW) and nutrients from the Mississippi and Atchafalaya Rivers resulting in wide-spread hypoxic conditions in bottom waters every summer. Nutrient inputs from the Mississippi River basin are estimated at about 1.2 million tons of nitrogen (N) and 0.15 million metric tons of phosphorus (P) per year (Aulenbach et al., 2007). The large N and P loads stimulate high rates of net primary production (NPP) on the shelf (Lohrenz et al., 1997), which fuels microbial respiration during organic matter decomposition. Vertical density stratification—a prerequisite for hypoxia development—is pronounced in spring and summer in parts of the NGoM, limiting the resupply of O_2 to bottom waters (Yu et al., 2015a). This strong stratification is largely due to the riverine FW inputs. A fraction of the FW flowing down the main stem of the Mississippi River is diverted to the Atchafalaya River by manmade structures (e.g. Allison et al., 2012), resulting in 30% of the upper Mississippi River flow being discharged by the Atchafalaya River (Rosenheim et al., 2013; Scavia et al., 2003). On the shelf, the distribution of FW constitutes the primary determinant of stratification and exhibits strong seasonal and inter-annual variations (Hetland & Zhang, 2017; Wiseman et al., 1997).

Systematic surveys of hypoxia have been conducted in the NGoM since 1985 (Rabalais et al., 1991) and show that, on average, hypoxia occupies an area of 15,000 ± 5,000 km^2 in mid-summer. This constitutes the largest hypoxic zone in North American coastal waters. The multi-state, multi-agency Mississippi River/Gulf of Mexico Hypoxia Task Force is charged with designing strategies for reducing the hypoxic zone through nutrient management in the watershed and, in 2001, the Task Force has set the goal of reducing the 5-year running

average size of the hypoxic zone to 5,000 km^2, i.e. a third of its current average size (Task Force, 2001). However, to date no measurable reduction has occurred (Task Force, 2017).

Significant progress has been made in quantifying the relative importance of different factors contributing to hypoxia formation and its temporal variability using a range of modeling approaches from purely statistical to high-resolution mechanistic models. Statistical models have linked the spatial extent of hypoxia to the riverine nutrient loads and have been used to predict hypoxic spatial extent (Scavia et al., 2017 and references therein). These models show that riverine May N load is a predictor of year-to-year variability in hypoxic area; however, because FW discharge and nutrient loads are highly correlated (Obenour et al., 2012) these analyses cannot differentiate between the effects of FW on stratification and nutrient inputs on O_2 consumption. In the statistical analysis of Forrest et al. (2011), total N load explained 24% of the year-to-year variations in the hypoxic area, while zonal wind speed explained 16%. Their analysis points to the important role of oceanographic processes in contributing to hypoxia variations in the NGoM.

Three-dimensional (3D) physical-biogeochemical models that are based on realistic coastal circulation models and include mechanistic descriptions of the most important biogeochemical processes affecting O_2 have been developed as well. These spatially explicit models enable a realistic representation of nutrient and O_2 dynamics and allow detailed analyses of the different causes of hypoxia. For the NGoM, at least four different coupled physical-biogeochemical models are currently available: the Regional Ocean Modeling System (ROMS; Fennel et al., 2011; Laurent et al., 2012), the Finite Volume Community Ocean Model (FVCOM; Justić & Wang, 2014), the Gulf of Mexico Dissolved Oxygen Model (GoMDOM; Pauer et al., 2016), and the Coastal General Ecosystem Model (CGEM; Lehrter et al., 2017).

In the ROMS model, which includes N- and P-based nutrients, P-limitation is simulated in spring and early summer, in agreement with observations (Sylvan et al., 2006), and influences the severity and distribution of hypoxia (Laurent & Fennel, 2014), but N is the ultimate limiting nutrient in the NGoM (Fennel & Laurent, 2018). Yu et al. (2015a, 2015b) quantified the influence of different physical and biogeochemical processes on O_2 dynamics with the same model and showed that sediment O_2 consumption (SOC) constitutes the largest O_2 sink in the bottom boundary layer, where hypoxia occurs.

These models have also been used to project future changes in O_2 conditions, e.g. under climate change or due to reductions in the riverine nutrient loads. An increase in spatial extent and severity of hypoxia is predicted to occur in the future due to reduced O_2 solubility

and increased stratification in a warmer climate (Laurent et al., 2018; Lehrter et al., 2017). Modeling studies on the effect of riverine N load reductions on hypoxia suggest that a reduction in the order of 60% would be sufficient to achieve the 5,000 km^2 management target (Fennel & Laurent, 2018) in agreement with results from statistical models (Scavia et al., 2017).

However, current models cannot quantify the relative importance of the three main nutrient sources, i.e. the Mississippi River, Atchafalaya River and the open ocean, which is important for the development of hypoxia mitigation strategies. FW contributions from individual riverine sources can be traced with passive dye tracers and, in combination with so-called age tracers (Deleersnijder et al., 2001; Ménesguen & Hoch, 1997), transit times from different sources can be quantified. Zhang et al. (2012) and Hetland & Zhang (2017) used passive FW tracers in the NGoM and showed that east of Atchafalaya Bay, stratification on the shelf is dominated by FW from the Mississippi River throughout the year. Farther west, FW from the Atchafalaya River dominates near-shore and forms a westward coastal jet except during periods of westerly, upwelling-favorable winds, when it extends farther offshore (Zhang et al., 2012). These different patterns of FW transport suggest that the relative influence of nutrients from the two rivers on NPP and O_2 consumption may also differ across the shelf. However, a quantitative analysis of the relative importance of nutrient inputs from the Mississippi and Atchafalaya Rivers versus those from offshore has not yet been done. Such a quantification has become more relevant in light of recent discussions to divert river discharge towards coastal wetlands in order to reduce nutrient loads into the NGoM (e.g., Allison & Meselhe, 2010; Peyronnin et al., 2017; White et al., 2018). An increased discharge diversion toward the Atchafalaya River would likely change spatial patterns of stratification and affect hypoxia formation.

The relative contribution of the different nutrient sources to biogeochemical fluxes can be diagnosed with the help of an active element tracing technique described by Ménesguen et al. (2006) and Große et al. (2017). Here we apply this technique to the physical-biogeochemical NGoM model described in Fennel et al. (2011, 2013) and Laurent et al. (2012). In addition, we estimate transit times of river inputs across the shelf with the help of age tracers (e.g. Deleersnijder et al., 2001; Ménesguen & Hoch, 1997).

2 Methods

2.1 The physical-biogeochemical model

We use a physical-biogeochemical model that has already been used extensively for the NGoM (see **Fig. 1a;** Fennel et al., 2011, 2013; Laurent et al., 2012, 2017, 2018; Yu et al., 2015b). The physical model component is based on ROMS (Haidvogel et al., 2008) and has been implemented and validated by Hetland & DiMarco (2008, 2012). The biogeochemical model component is based on the N-cycle model of Fennel et al. (2006, 2008) but was expanded to include phosphate as additional nutrient (Laurent et al., 2012). The model state variables include nitrate (NO_3), ammonium (NH_4), phosphate (PO_4), one functional group each for phyto- and zooplankton, and three groups of detritus (small, large and river detritus), and dissolved oxygen (see **Fig. 1b**). The non-sinking river detritus was implemented by Yu et al. (2015b) in order to account for terrestrially derived dissolved organic matter which is respired more slowly than small marine detritus. The complete set of the model equations and parameter settings is given in Laurent et al. (2017), except for the sediment-water fluxes for which we use the instantaneous remineralization parameterization of Fennel et al. (2006, 2011). SOC is calculated from the benthic remineralization fluxes of small (BR_{SDetN}) and large detritus N (BR_{LDetN}) and phytoplankton N (BR_{PhyN}) using a molar ratio of O_2 consumption to NH_4 release of 115:4:

$$\mathrm{SOC} = \frac{115\ mol\ O_2}{4\ mol\ N} \times (\mathrm{BR}_{SDetN} + \mathrm{BR}_{SDetN} + \mathrm{BR}_{PhyN}). \quad (1)$$

The model has previously demonstrated good skill in reproducing spatial patterns and seasonal cycles of nitrate, phosphate, chlorophyll-a, bottom O_2 and rates of PP and respiration (Fennel et al., 2011; Laurent et al., 2012; Yu et al., 2015b), although it is known to slightly overestimate bottom O_2 concentrations and thus to underestimate hypoxia (Fennel et al., 2013; Yu et al., 2015b).

The model is forced with 3-hourly winds from the North American Regional Reanalysis model (NARR; Mesinger et al., 2006)) and climatological surface heat and FW fluxes from Da Silva et al. (1994a, 1994b), daily FW discharge estimates for the Mississippi and Atchafalaya Rivers from the U.S. Army Corps of Engineers at Tarbert Landing and Simmesport, respectively, and riverine loads of NO_3, NH_4 and PO_4, and particulate and dissolved organic matter from the U.S. Geological Survey (Aulenbach et al., 2007). At the open boundaries, monthly climatological concentrations of temperature, salinity, NO_3, NH_4, PO_4, and O_2 are prescribed, based on the World Ocean Atlas 2009. Boundary concentrations

of all other biogeochemical tracer variables are set to small positive values. The model was run for the years 2000 to 2011, but the first year is considered as spin-up and only subsequent years are used in the analyses herein.

2.2 Passive dye and age tracing

Dye and age tracers were implemented to track the transport pathways of FW from the Mississippi and Atchafalaya Rivers similar to previous ROMS applications (Hetland & Zhang, 2017; Rutherford & Fennel, 2018; Zhang et al., 2010, 2012). This requires two additional tracers for each FW source: a passive dye and an active age tracer that keeps track of the "aging" of each dye since it departed from its source.

The rate of change of a passive dye tracer (C_p) is described by the advection-diffusion equation:

$$\frac{\partial C_p}{\partial t} = \nabla \cdot \left(\overline{\overline{D}} \nabla C_p\right) - \nabla \cdot \left(C_p \vec{v}\right) + S_{C_p}, \tag{2}$$

where $\overline{\overline{D}}$ is the second order diffusion tensor (or diffusivity) and $\vec{v}$ the 3-D velocity vector. S_{C_p} represents the external dye tracer sources (e.g. river FW discharge).

Age (τ) can be thought of as the time it took a water parcel to travel from its source to a specific location. Considering each water parcel as a mixture of different sources and ages implies a distribution of ages at each point in space and time and for each dye tracer. Following Delhez et al. (1999), the dye tracer concentration, C_p, is represented by:

$$C_p = \int_0^\infty c_p(\tau)\, d\tau, \tag{3}$$

where $c_p(\tau)$ is the concentration of the passive dye tracer of age τ. Analogously, the age concentration associated with the dye tracer reads as:

$$\alpha_p = \int_0^\infty \tau c_p(\tau)\, d\tau. \tag{4}$$

The rate of change of the age concentration is calculated as:

$$\frac{\partial \alpha_p}{\partial t} = \nabla \cdot \left(\overline{\overline{D}} \nabla \alpha_p\right) - \nabla \cdot \left(\alpha_p \vec{v}\right) + C_p. \tag{5}$$

Equation (5) is linked to Eq. (2) such that α_p increases with each time step if $C_p > 0$.

Then the mean age of a dye tracer at a given location and time (x, y, z, t) is calculated as the mass-weighted average of the age concentration (Deleersnijder et al., 2001):

$$a_p = \frac{\alpha_p}{C_p}. \tag{6}$$

For a more detailed description, see Deleersnijder et al. (2001) and Rutherford & Fennel (2018).

For our simulations, the FW dye and age tracers are initialized at zero. The dye tracer concentrations in their corresponding rivers are 1. The concentrations inside the domain start increasing when FW from the Mississippi and Atchafalaya Rivers enters the domain. At the open boundaries, both tracers are set to zero, i.e. the information on source and age of FW is lost when it leaves the domain.

2.3 Active nitrogen tracing

In addition to the tracing of FW sources and ages, active element tracing is implemented to track how N from distinct sources is travelling through the region and the different biogeochemical compartments. This requires tracking of biogeochemical transformations as well. Conceptually, the tracing of N from individual sources is comparable to isotopic labeling. Each state variable is the sum of fractions that are labeled according to their sources. Sources can be point sources (e.g. rivers) or defined regions within the model domain (e.g. the open Gulf/open boundaries).

The governing equation for the rate of change of a specific source fraction reads similar to Eq. (2) but with the addition of a term for biogeochemical sources and sinks. We apply the approach described by Große et al. (2017):

$$\frac{\partial c_X^i}{\partial t} = \nabla \cdot \left(\overline{\overline{D}} \nabla C_X\right) \cdot \frac{c_X^i}{c_X} - \nabla \cdot (\vec{v} C_X) \cdot \frac{c_X^i}{c_X} + R_{C_X} \cdot \frac{c_{X_{con}}^i}{c_{X_{con}}}, \tag{7}$$

where C_X represents the concentration of the state variable X (e.g. NO_3) and C_X^i is its labeled fraction from the i-th source (e.g. NO_3 from the Mississippi River). R_{C_X} describes internal and external sources and sinks of X. Equation (7) shows that the processes acting on the source-specific fractions are calculated as the product of the processes acting on each state variable (e.g. NO_3 uptake during NPP) and the relative concentration of its labeled fraction. For the diffusion term, this approach differs slightly from other studies that used the concentration gradient of the source-specific fractions instead of that in the state variable (Ménesguen et al., 2006; Ménesguen & Hoch, 1997; Radtke et al., 2012; Troost et al., 2013). The index 'con' in the source/sink term indicates that the relative concentration of the variable that is consumed by a process is used. For instance, the source-specific nitrification flux to NO_3 is calculated based on the relative concentration of NH_4. When tracing multiple different sources, one set of equations (i.e. one for each state variable) of the form of Eq. (7)

needs to be solved for each source. This is illustrated schematically by the different colors in **Fig. 1b**.

For this purpose, the element tracing software (ETRAC) by Große et al. (2017) was adapted to ROMS. It requires model output for all N cycle sources and sinks (i.e. all physical and biogeochemical processes) to fulfill the following criterion for all state variables X:

$$V(t+\Delta t)\cdot C_X(t+\Delta t) - V(t)\cdot C_X(t) = \sum_{j=1}^{N} P_{X,j}(\Delta t). \quad (8)$$

Here, V represents the volume of a model grid cell, Δt is the model's output time step, and P_X are the N processes that affect X cumulated over Δt. In other words, the change in mass of X, calculated as the sum of all processes cumulated over Δt, must be exactly the same as the change in mass calculated as the difference between the masses at the beginning and end of each output time step. The necessary model output was stored daily (tracer concentrations at midnight; daily cumulated fluxes) and then used as input for ETRAC.

Although our model includes N- and P-based nutrients and simulates P-limitation over parts of the shelf in spring and early summer, we apply the element tracing to N only, since it is the ultimate limiting nutrient in the NGoM (Fennel & Laurent, 2018; Rabalais et al., 2002b). N from three different sources, the Mississippi and Atchafalaya Rivers, and the inflow across the open boundary (see colors in **Fig. 1b**) is traced. Riverine N enters the domain according to the river input fluxes of the N tracers. All mass entering the domain across the open boundary is attributed to this source, i.e. riverine N tracers cannot reenter the domain. At initialization, all mass of N tracers inside the domain was arbitrarily attributed to Mississippi River. A 2-year spin-up was conducted for the year 2000 by repeating its forcing once. Comparison of the relative contributions of all N tracers at the end of both spin-up years confirmed that a statistical steady state is reached after one year, i.e. differences between the two years were negligible. We then simulated the years 2001 to 2011, referred to as the control. The daily output of ETRAC provides the source-specific fluxes and tracer concentrations used for the calculation of the contributions to TN, NPP and SOC. Source-specific SOC is calculated using Eq. (1) and the source-specific benthic remineralization fluxes.

2.4 Model scenarios

In addition to the control simulation (see **Sect. 2.1**), we conducted four different scenario simulations: two N load reduction scenarios where riverine N input was reduced by 20% and 60%, a discharge diversion scenario with an equal FW distribution between the Mississippi

and Atchafalaya Rivers, instead of the current 7:3 distribution, and a combined 60% riverine N load reduction and 1:1 discharge distribution scenario.

The 20% reduction corresponds to the interim target defined by the Task Force (2014), whereas the 60% reduction is the estimated reduction necessary to reach the 5,000 km^2 target for the hypoxic zone (Fennel & Laurent, 2018; Scavia et al., 2017). In both cases, river forcing is as in the control simulation, except that the riverine concentrations of the N-related state variables are multiplied by 0.8 or 0.4.

In the first diversion scenario with altered FW distribution between the Mississippi and Atchalafaya Rivers only, we change the discharge. Riverine N concentrations are as in the control simulation. This discharge diversion results in a 2.5% reduction of the overall TN load due to slightly lower N tracer concentrations in the Atchafalaya River, resulting from a more efficient filtering of terrestrial N inputs by Atchafalaya wetlands. In the combined N load reduction and diversion scenario, the FW discharge is changed and the riverine concentrations of all N-related state variables are multiplied by 0.4. All scenarios are run for 2000 to 2011, with the year 2000 used as spin-up. The element tracing is only applied to the years 2000 and 2001 of the two N reduction scenarios, with year 2000 used as spin-up.

3 Results

3.1 Riverine nitrogen loads

The daily climatological loads of total nitrogen (TN) from the Mississippi and Atchafalaya Rivers, calculated over the simulation period, and the daily loads for the years with the smallest (2003) and largest (2008) observed hypoxic area during the simulation period are shown in **Fig. 2**. The climatologies for both rivers exhibit a distinct seasonal cycle that mainly reflects the seasonal cycle of FW discharge. Highest loads usually occur in May/June, while loads are lowest in September/October. The large standard deviations of the climatologies and the two individual years indicate that the inter-annual variability in TN loads (and FW discharge) is high.

The TN loads of the Mississippi River are consistently about 2.5 times higher than those of the Atchafalaya River, a direct result of the 7:3 discharge distribution between the two rivers. This suggests a higher contribution of Mississippi N to NPP and SOC. However, the influence of these loads on shelf biogeochemistry does not only depend on the overall load but also on the residence time of the nutrients on the shelf. The next section provides

information on the spatial distributions of FW from the Mississippi and Atchafalaya Rivers on the shelf and estimates of their transit times.

3.2 Freshwater thicknesses and transit times

For the representation of FW distributions from the Mississippi and Atchafalaya Rivers we use the FW thickness defined by Zhang et al. (2012) as:

$$h_{fw} = \int_{-H}^{\eta} C_p \, dz, \tag{9}$$

where η and H are the sea surface elevation and bathymetric depth at (x, y, t), respectively.

The average spatial distribution of the FW thicknesses from both rivers between June and August is shown in **Fig. 3**. Mississippi FW dominates the shelf with a FW thickness >2 m east of 91°W and about 1.5 m along the 25 m isobath off and west of Atchafalaya Bay (see **Fig. 3a**). Regions of high Atchafalaya FW thickness (>1.5 m) are confined to a narrow coastal band stretching westward from Atchafalaya Bay (see **Fig. 3b**). This indicates that the Mississippi River discharge is the main control of stratification on the shelf during summer.

These simulated distributions of FW thickness agree well with those of Zhang et al. (2012) from a higher resolution model with a larger domain. Expanding upon their work, we can use the mean ages of FW to determine its transit times from the source to each location within the domain. The mean age of Mississippi FW (**Fig. 3c**) continuously increases from east to west reflecting the westward transport on the shelf. The FW transit time from the Mississippi delta to the western model boundary is 2.5-3 months. The mean age of Atchafalaya FW (**Fig. 3d**) is much lower (< 1 month), especially in regions with high Atchafalaya FW thickness; in other words, Atchafalaya River discharge quickly leaves the domain across the western boundary. The longer transit times of Mississippi FW suggest that its N loads may reside longer and can be recycled more frequently in the region west of the Mississippi River Delta.

3.3 Influence of nitrogen sources under realistic environmental conditions

Next, we present the average spatial patterns of TN, NPP and SOC on the shelf, and the relative contributions from the three different N sources. As wind forcing has been shown to strongly influence FW dispersal on the shelf (Zhang et al., 2012), we also analyze the effect of the wind field on these spatial patterns.

First, we provide the 11-year average spatial patterns of vertically averaged TN, of vertically integrated NPP, and of SOC during summer (June-August; **Fig. 4a-c**), and the relative contributions to TN by the Mississippi and Atchafalaya Rivers (**Fig. 4d, e**). The values for TN and NPP are calculated over a depth range of 0-25 m (to the bottom in

shallower regions). The relative contributions to NPP and SOC are very similar to those to TN, hence not shown. The relative contribution of N from the open boundary is small (<15%) in most regions shallower than 50 m.

The spatial distribution of the relative contributions of both rivers is similar to its corresponding FW thickness (**Fig. 3a, b**). This suggests that the different FW transit times (**Fig. 3c, d**) are transferable to riverine N and, thus, that Mississippi N spends more time in the region experiencing hypoxia.

TN, NPP and SOC on the eastern and central shelf are dominated by Mississippi N, which contributes >70% east of 91°W (**Fig. 4d**; shown for TN only). On the western shelf, Atchafalaya N (**Fig. 4e**) constitutes the main contribution in the near-shore regions but steadily decreases in importance toward the middle and outer shelf and is below 30% in most regions deeper than 25 m, while the Mississippi contribution increases and extends far toward the west. The Mississippi contribution has its cross-shelf maximum (>50% east of 94°N) roughly centered on the 25-m isobaths. N from the Mississippi River dominates productivity in most of the shelf regions during summer, except for the narrow coastal band west of Atchafalaya Bay. The spatial patterns of the average relative contributions of the Mississippi and Atchafalaya Rivers (**Fig. 4d, e**) reflect the predominantly easterly, downwelling-favorable winds in the region (Feng et al., 2014).

Next, we analyze the effect of westerly, upwelling-favorable winds on the contributions to NPP on the shelf. This effect is illustrated by the daily time series of source-specific vertically integrated NPP at station C6C (see **Fig. 1a**) averaged over 2001-2011 and in 2009 (see **Fig. 5**). This provides insight in the average seasonality of the different contributions to NPP compared to a year with sustained upwelling-favorable wind conditions (Laurent et al., 2018). Periods of upwelling-favorable conditions are derived from spatially averaged, daily zonal wind speed and are indicated at the top of each panel (see **Fig. 1a** for averaging region).

On average, the Mississippi contribution is the dominant one throughout the seasonal cycle at station C6C (**Fig. 5a**). That of the Atchafalaya is close to zero, except from late May through September, when recurring upwelling-favorable winds support the eastward transport of Atchafalaya N. Concurrently, total NPP and its contributions from the Mississippi and the open ocean decrease, indicating an offshore displacement of N from these sources. In 2009 (Figure 5**b**), the temporal evolution of the different contributions from January to May is similar to the 11-year average. A period of sustained upwelling-favorable winds from early June to early August results in a significant increase in the Atchafalaya contribution causing an increase in total NPP to its 2009 maximum. Similar to the 11-year average, the Mississippi

and the open-ocean contributions drop to about half of their spring contributions during this period. The relatively high standard deviations of the 11-year average (shaded areas in **Fig. 5a**) and the special case of 2009 further suggest that interannual variability is high especially in the riverine contributions. This illustrates that the zonal wind field has a significant impact on the contributions of the individual N sources to NPP as it controls the dispersal of their inputs on the shelf.

Next, we assess whether some N sources are more important to SOC and hypoxia generation than others. The contributions of the different N sources to SOC during summer, when hypoxia is most pronounced, are quantified in **Fig. 6**. In order to relate them to hypoxic extent, we also show the hypoxic area estimates from Obenour et al. (2013). On average, 51±9% and 33±9% of summer SOC can be attributed to Mississippi and Atchafalaya N, respectively. Both N loads together support 84±2% of total summer SOC on the shelf. N from the open boundary supports the remaining 16±2%. For comparison, the net input of open-ocean N onto the shelf (0-25 m depth) is about 23±4% of the combined riverine inputs directly discharged into the region. The small standard deviation in the combined riverine contribution indicates that the balance between the two riverine sources controls summer SOC on the shelf.

Inter-annual variability in the individual riverine contributions is high. The Mississippi contribution varies between 39% (2009) and 64% (2007), while that of the Atchafalaya River varies between 17% (2001) and 43% (2009). Large hypoxic areas usually occur during years of high contributions from the Mississippi River. This is emphasized by the qualitative relationship between the anomalies of the Mississippi contribution to SOC and the anomalies of the hypoxic area extent (see Supplement: **Text S1** and **Fig. S1**), while no such relationship is found for the Atchafalaya contribution to SOC. **Figure 6** further shows that, despite episodic increases in NPP during upwelling-favorable wind events in 2009 (see **Fig. 5b**), total SOC is lowest during years of sustained upwelling-favorable winds (2005 and 2009).

It is worth mentioning that the importance of the Mississippi River increases relative to that of the Atchafalaya River when considering the regions with depths up to 50 m (see Supplement: **Text S2, Tables S1** and **S2**, and **Fig. S2**). This relates to the higher Mississippi contributions offshore (see **Fig. 4d**).

In order to investigate the effect of differences in transit time (see **Fig. 3**), we define the 'influence' of an N source as the ratio of its source-specific SOC on the shelf to its N load. In other words, the 'influence' measures how much SOC is generated per unit N load from each source. **Figure 7** shows the 2001-2011 annual time series of SOC per unit of N input from

both rivers and the open ocean (i.e. the 'influence') for the entire year (dark colors) and during summer (May-August; light colors) in the domain west of the Mississippi River Delta. Mississippi N consistently has a higher influence than Atchafalaya N, ranging from 1.4-fold in 2006 to 4.5-fold in 2002, due to its longer transit time along the shelf. The influence of both rivers' loads increases further during summer, in some years significantly. During years with strong upwelling events (e.g., 2005 and 2009) the influence of the Atchafalaya N load can be on the same order as that of the Mississippi. The influence of the open-ocean input consistently is less than 0.07 mol O_2 (mol N)$^{-1}$), demonstrating that, despite large open-ocean N inputs into the model domain, their contribution to hypoxia formation is small.

3.4 Effects of riverine N load reductions

Next, we analyze the effects of riverine N load reductions by 20% and 60% on the source-specific contributions to TN, NPP and SOC, and on the hypoxic area (**Table 1**). In both scenarios, the simulated reductions in pelagic TN concentration exceed the applied N load reductions. The simulated reductions in NPP and SOC for a 60% reduction in N load are 32.5% and 34.8%, respectively, i.e. clearly lower than those in the N loads. Reductions in NPP and SOC supported by Mississippi N are largest (40.8% and 41.8%, respectively) due to the higher influence of Mississippi N on the shelf. The response in hypoxic area is only 6.9% for the 20% load reduction, but a 47.6% reduction is achieved under a 60% reduction.

NPP and SOC per unit river load increase significantly under reduced N loads. In other words, relatively less N is required to fuel the same amount of NPP and SOC, explaining the lack of a proportional response to N load reductions. This is most pronounced in the river plumes, where NPP is highest, while reductions in NPP are high only in the less productive regions further downstream (see Supplement **Text S3** and **Fig. S3** for more details). In our model, SOC is directly proportional to benthic denitrification (Fennel et al., 2013). Hence, the increase in SOC per unit river load implies a faster removal of riverine N from the system via benthic denitrification as a result of the very limited response of NPP to N load reductions in the most productive regions. This also explains why simulated reductions in the pelagic concentrations of TN from the two rivers exceed the reductions in their N loads. Changes in SOC, bottom O_2 and hypoxic exposure for a 60% N load reduction are shown in **Fig. 8a-c** relative to the control simulation averaged over June to August 2001-2011. Simulated SOC is reduced in all regions shallower than 50 m (**Fig. 8a**). As suggested by the analysis above, reductions in SOC are lowest closest to the river mouths and stay below 2 mmol O_2 m^{-2} d^{-1} east of 90°W, but stronger reductions occur farther west. Bottom O_2 concentrations show the

strongest increase on the western shelf and in the shallow area south of Terrebonne Bay (**Fig. 8b**). Accordingly, reductions in hypoxic exposure are highest in these regions with values of two to three weeks (**Fig. 8c**).

Next, we investigate whether a 1:1 discharge distribution, which significantly affects distributions of both nutrients and FW, could lead to stronger improvements near the river mouths and complement N load reductions to mitigate hypoxia.

3.5 Effects of a river discharge diversion

First, we analyze the changes in SOC, bottom O_2 and hypoxic exposure for the discharge diversion scenario (**Figs. 8d-f**). Changes in SOC mostly reflect the changes in nutrient input due to the diversion, i.e. a minor decrease (increase) occurs in most regions east (west) of 91.5°W (**Fig. 8d**). Directly at the river mouths, the change in SOC is opposed to the change in discharge, i.e. SOC increases at the Mississippi River mouth and decreases off Atchafalaya Bay; an effect of light availability, which includes a salinity-dependent term in our model (Green et al., 2008). The changes in bottom O_2 concentration and hypoxic exposure (**Figs. 8e**, **f**) reflect the changes in both SOC and stratification (represented by potential energy anomaly; Simpson, 1981) in most regions (see Supplement, **Fig. S4**). Near the river mouths, changes in bottom O_2 and hypoxic exposure are primarily driven by changes in stratification. It should be noted that averaged over the shelf, changes in bottom O_2 and hypoxic exposure are negligible.

Figure 8a-f show that the 60% N load reduction alone supports stronger improvements in the bottom O_2 conditions in the west, while the 1:1 discharge distributions results in improvements in the east and a slight deterioration in the west. To investigate whether a combined 60% N load reduction and discharge diversion could result in a stronger shelf-wide improvement, **Figs. 8g-i** show the simulated changes in SOC, bottom O_2 and hypoxic exposure for this combined scenario. East of 90.5°W the simulated reductions in hypoxic exposure exceed those in the reduction-only scenario (compare **Figs. 8c** and **i**). However, elsewhere, the improvements are less than for the load reduction. In other words, the combination of load reduction and discharge diversion results in a weaker response and larger hypoxic areas than the reduction-only scenario (see **Table S3**).

4 Discussion

The Mississippi River's TN loads are about 2.5 times higher than those of the Atchafalaya River (see **Fig. 2**) primarily due to the current 7:3 discharge distribution between the two

rivers. Predominantly westward winds cause a westward transport of these river inputs resulting in a large area of influence of Mississippi N on the northern Gulf of Mexico shelf (see **Figs. 3** and **4**, respectively). On average, Mississippi N contributions to summer TN, NPP and SOC are above 50% in the studied shelf region, while Atchafalaya N only has a high contribution in a narrow coastal band off and west of Atchafalaya Bay. Only during events of sustained upwelling-favorable (eastward) winds, does Atchafalaya N reach the eastern shelf and fuel local increases in NPP (**Fig. 5**). Our analysis suggests that Mississippi River, Atchafalaya River and open-ocean N support 51±9%, 33±9% and 16±2%, respectively, of summer SOC in the region most affected by hypoxia (2001-2011 averages; **Fig. 6**). The Mississippi River constitutes the main control of O_2 consumption in the NGoM because of the predominantly westward transport of river water.

Our results indicate that Mississippi River water needs ~3 months, 2-3 times longer than Atchafalaya water, to reach the western boundary of the model domain and leave (**Fig. 3**). This allows for a more frequent recycling of Mississippi River N, resulting in 1.4 to 4.5-times higher SOC per unit of riverine N load averaged over the year (**Fig. 7**).

Feng et al. (2014) showed that the wind forcing during summer has a significant impact on water mass transport and hypoxia on the shelf. Episodes of eastward, upwelling-favorable winds cause an eastward and offshore transport on the shelf. This is visible in the significant increase in the contribution of Atchafalaya N to NPP at station C6C on the eastern shelf in 2009 (**Fig. 5**) during an unusual and prolonged period of eastward winds. During such events, the contribution of Atchafalaya N to SOC increases and is visible even in the annual averages (**Fig. 7**). However, total shelf-wide SOC is lower in years of sustained upwelling-favorable conditions (**Figs. 6** and **S2**) as less Mississippi N is retained on the shelf. This is in line with the observations of Huang et al. (2015), who found less NPP in 2009 (strongly upwelling-favorable) than in 2007 (no upwelling).

The consistently small contributions of oceanic N to SOC (16±2%; see **Fig. 6**) are not surprising given the nutrient-poor surface waters in the oligotrophic open Gulf (e.g. Strom & Strom, 1996). The deep nutricline (~300 m; Gomez et al., 2018) in the open Gulf inhibits upwelling of nutrient-rich water onto the shelf. In addition to the small influx of open-ocean nutrients, their SOC per unit of N influx is small (< 0.07 mol O_2/mol N; see **Fig. 7**).

The size of the combined contribution of riverine N loads to SOC (84±2%) shows clearly that they are the main control of O_2 consumption. Fennel & Laurent (2018) recently showed that reductions in riverine N loads translate into smaller than proportional NPP reductions in the NGoM. Our results show that nonlinear responses result in significant spatial differences

in how NPP responds to altered nutrient inputs. Near the Mississippi River Delta, in the most productive shelf region, the portion of NPP fueled by Mississippi N is reduced by less than 15% in the 60% N-load reduction (see **Figs. S3a**, **b**) because of improved light availability (see **Fig. S3d**) and the fact that N supply is so excessive that P limitation occurs in these regions (Fennel & Laurent, 2018; Laurent et al., 2012). In contrast, large reductions in the portion of NPP fueled by Mississippi N, of up to 80%, occur in regions farther downstream (west) where hypoxia is less likely to occur. Similar spatial differences are simulated for NPP fueled by Atchafalaya N. Due to these spatial differences, the shelf-wide averaged reductions in NPP and SOC in 2001 are only 33% and 35% under a 60% N load reduction (see **Table 1).**

With respect to hypoxia mitigation, our results suggest that a 60% reduction in riverine N loads is preferable over a combined 60% N load reduction and 1:1 discharge distribution between the Mississippi and Atchafalaya Rivers (see **Fig. 8** and **Table S3**). The N load reduction alone results in significant reductions in hypoxic exposure (~2-3 weeks) in most regions downstream from the immediate vicinity of the river mouths. An additional discharge redistribution only results in improvements east of 91°W, but not on the rest of the shelf due to higher SOC and a westward shift in stratification (see **Fig. S4**). The weaker response west of 91°W outweighs the improvement in the east, resulting in an overall lower reduction of hypoxia than in the N load reduction case.

The ROMS model used here constitutes a well validated modeling framework, which has previously demonstrated good skill in reproducing both the physical (Hetland & DiMarco, 2012) and the biogeochemical (Feng et al., 2014; Fennel et al., 2011, 2013) environment of the NGoM. Hetland & DiMarco (2012) showed that the model captures temperature and salinity distributions, current velocities and large-scale circulation features, and found that small-scale features (e.g. eddies) along the shelf break are statistically reproduced. Fennel et al. (2013) and Marta-Almeida et al. (2013) further demonstrated that the model captures the main features of the shelf hydrography and oxygen dynamics when using climatological boundary conditions, despite differences in freshwater fluxes across the model's southern boundary. The applied element tracing method can be described as a non-disruptive method (Ménesguen & Lacroix, 2018), not affecting the balance between different nutrient sources and biogeochemical processes. Hence, it allows for the quantification of the contributions of individual nutrient sources under realistic environmental conditions.

The application of this active N tracing in concert with the passive FW and age tracers allows for the estimation of transit times of riverine N inputs on the shelf with comparably little computational effort. Only one pair of additional passive tracers (FW and age) is needed

for each riverine source, while direct age tracing for the source-specific riverine N tracers would increase the computational costs by a factor of 7, i.e., the number of N tracers in the model. Despite these advantages, some limitations of the applied setup need to be discussed.

With respect to our model, it is known that it slightly underestimates near-bottom hypoxia due to underestimated SOC (Fennel et al., 2013). However, as the relative contributions of the different N sources to the biogeochemical processes only depend on their relative distribution in the system and not on the magnitude of the benthic processes, we are confident that this does not affect our results. Some empirical parameterizations of benthic processes have shown better agreement with observations (Hetland & DiMarco, 2008; Laurent et al., 2016). However, those do not allow for the application of the active element tracing as it requires process-based, mass-conservative formulations of the biogeochemical processes of the labeled element.

With respect to the FW and N tracing, the treatment of the open boundaries implies that the information on the riverine origin is lost when a tracer leaves the model domain across the open boundary. Consequently, the contribution of the Atchafalaya River might be slightly higher than our analysis suggests, especially in the far west of the domain, where summer events of westerly winds can cause significant eastward flow. Similarly, the contribution of the Mississippi River may be slightly higher during periods of easterly winds, due to recirculation of FW and N that left the domain across the southern boundary.

In relation to our discharge diversion scenario, it is important to note that the diversion from the Mississippi River towards the Atchafalaya River applied here may not be practical and differs from potential diversions investigated in other studies (e.g. Allison & Meselhe, 2010; Peyronnin et al., 2017) and considered by Louisiana's Coastal Protection and Restoration Authority (CPRA, 2017). The latter consider diversions of water from both Mississippi and Atchafalaya Rivers towards wetlands, such as Barataria Bay or Terrebonne Bay. Nevertheless, an investigation of the diversion applied here is a useful test case for assessing potential shelf-wide effects.

5 Conclusions

This study presents the first application of active tracing of N and FW age for the individual inputs from the Mississippi and Atchafalaya Rivers in a model for the NGoM. This allowed to quantify the relative contributions of the individual N sources to NPP and SOC in a spatially explicit manner.

In the regions that are most susceptible to hypoxia, Mississippi and Atchafalaya N on average support 51% and 33% of SOC during June to August 2001–2011, respectively. About 2.5 times higher loads and more frequent recycling of N from the Mississippi River, due to 2-3 times longer transit times, are the main causes for these different contributions. The combined riverine contribution of 84% emphasizes the high potential of riverine N reductions to mitigate hypoxia on the shelf. However, the response in NPP to N reductions is strongly nonlinear causing reductions in NPP and SOC to be lower than the load reductions especially in the river plumes, which are the most productive regions. Consequently, simulated NPP and SOC reductions on the shelf result in only 33% and 35% under a 60% N load reduction, respectively.

Our study suggests that a discharge diversion from the Mississippi River towards the Atchafalaya River could result in a westward shift of hypoxia, while it would not improve the shelf-wide O_2 conditions. Furthermore, a combined riverine N load reduction and 1:1 discharge distribution appears to be less effective in mitigating hypoxia than an N load reduction alone.

6 Acknowledgements

This study benefitted significantly from the MatLab toolboxes for TEOS-10 (McDougall & Barker, 2011) and the 'cmocean' color schemes (Thyng et al., 2016), whose authors are thankfully acknowledged. We thank Compute Canada for providing computing resources under the resource allocation project qqh-593-ac. K.F. acknowledges funding from the Natural Sciences and Engineering Research Council of Canada (NSERC) Discovery program. This work was supported by NOAA CSCOR grants NA06N0S4780198 and NA09N0S4780208. NGOMEX publication number XXX.

7 Data availability

A modified version of the ROMS source code that facilitates writing of model diagnostics needed by ETRAC is available at: https://github.com/FabianGrosse/ROMS_3.7_for_ETRAC. ETRAC can be accessed via: https://github.com/FabianGrosse/ETRAC. Data for all figures are provided in the supplementary materials. Original model output can be downloaded from: http://memg.ocean.dal.ca/grosse/shared_data/Grosse_etal_2019_JGR-Oceans.

8 References

Allison, M. A., & Meselhe, E. A. (2010). The use of large water and sediment diversions in the lower Mississippi River (Louisiana) for coastal restoration. *Journal of Hydrology*, *387*(3), 346–360. https://doi.org/10.1016/j.jhydrol.2010.04.001

Allison, M. A., Demas, C. R., Ebersole, B. A., Kleiss, B. A., Little, C. D., Meselhe, E. A., et al. (2012). A water and sediment budget for the lower Mississippi--Atchafalaya River in flood years 2008--2010: Implications for sediment discharge to the oceans and coastal restoration in Louisiana. *Journal of Hydrology*, *432-433*, 84–97. https://doi.org/10.1016/j.jhydrol.2012.02.020

Aulenbach, B. T., Buxton, H. T., Battaglin, W. A., & Coupe, R. H. (2007). *Streamflow and nutrient fluxes of the Mississippi-Atchafalaya River Basin and subbasins for the period of record through 2005*. https://doi.org/10.3133/ofr20071080

Breitburg, D., Levin, L. A., Oschlies, A., Grégoire, M., Chavez, F. P., Conley, D. J., et al. (2018). Declining oxygen in the global ocean and coastal waters. *Science*, *359*(6371). https://doi.org/10.1126/science.aam7240

CPRA. (2017). *Louisiana's Coastal Master Plan for a Sustainable Coast*. Baton Rouge, LA, USA. Retrieved from http://coastal.la.gov/wp-content/uploads/2017/04/2017-Coastal-Master-Plan_Web-Book_CFinal-with-Effective-Date-06092017.pdf

Deleersnijder, E., Campin, J.-M., & Delhez, E. J. M. (2001). The concept of age in marine modelling: I. Theory and preliminary model results. *Journal of Marine Systems*, *28*(3), 229–267. https://doi.org/10.1016/S0924-7963(01)00026-4

Delhez, E. J. M., Campin, J.-M., Hirst, A. C., & Deleersnijder, E. (1999). Toward a general theory of the age in ocean modelling. *Ocean Modelling*, *1*(1), 17–27. https://doi.org/10.1016/S1463-5003(99)00003-7

Díaz, R. J., & Rosenberg, R. (1995). Marine benthic hypoxia: a review of its ecological effects and the behavioural responses of benthic macrofauna. *Oceanography and Marine Biology: An Annual Review*, *33*.

Díaz, R. J., & Rosenberg, R. (2008). Spreading Dead Zones and Consequences for Marine Ecosystems. *Science*, *321*(5891), 926–929. https://doi.org/10.1126/science.1156401

Feng, Y., Fennel, K., Jackson, G. A., DiMarco, S. F., & Hetland, R. D. (2014). A model study of the response of hypoxia to upwelling-favorable wind on the northern Gulf of

Mexico shelf. *Journal of Marine Systems*, *131*(Supplement C), 63–73. https://doi.org/10.1016/j.jmarsys.2013.11.009

Fennel, K., & Laurent, A. (2018). N and P as ultimate and proximate limiting nutrients in the northern Gulf of Mexico: implications for hypoxia reduction strategies. *Biogeosciences*, *15*(10), 3121–3131. https://doi.org/10.5194/bg-15-3121-2018

Fennel, K., & Testa, J. M. (2019). Biogeochemical Controls on Coastal Hypoxia. *Annual Review of Marine Science*, *11*(1), 105–130. https://doi.org/10.1146/annurev-marine-010318-095138

Fennel, K., Wilkin, J., Levin, J., Moisan, J., O'Reilly, J., & Haidvogel, D. (2006). Nitrogen cycling in the Middle Atlantic Bight: Results from a three-dimensional model and implications for the North Atlantic nitrogen budget. *Global Biogeochemical Cycles*, *20*(GB3007), 1–14. https://doi.org/10.1029/2005GB002456

Fennel, K., Wilkin, J., Previdi, M., & Najjar, R. (2008). Denitrification effects on air-sea CO2 flux in the coastal ocean: Simulations for the northwest North Atlantic. *Geophysical Research Letters*, *35*(24), 1–5. https://doi.org/10.1029/2008GL036147

Fennel, K., Hetland, R., Feng, Y., & DiMarco, S. (2011). A coupled physical-biological model of the Northern Gulf of Mexico shelf: model description, validation and analysis of phytoplankton variability. *Biogeosciences*, *8*(7), 1881–1899. https://doi.org/10.5194/bg-8-1881-2011

Fennel, K., Hu, J., Laurent, A., Marta-Almeida, M., & Hetland, R. (2013). Sensitivity of hypoxia predictions for the northern Gulf of Mexico to sediment oxygen consumption and model nesting. *Journal of Geophysical Research: Oceans*, *118*(2), 990–1002. https://doi.org/10.1002/jgrc.20077

Forrest, D. R., Hetland, R. D., & DiMarco, S. F. (2011). Multivariable statistical regression models of the areal extent of hypoxia over the Texas{\textendash}Louisiana continental shelf. *Environmental Research Letters*, *6*(4), 45002. https://doi.org/10.1088/1748-9326/6/4/045002

Gomez, F. A., Lee, S.-K., Liu, Y., Hernandez Jr., F. J., Muller-Karger, F. E., & Lamkin, J. T. (2018). Seasonal patterns in phytoplankton biomass across the northern and deep Gulf of Mexico: a numerical model study. *Biogeosciences*, *15*(11), 3561–3576. https://doi.org/10.5194/bg-15-3561-2018

Gray, J. S., Wu, R. S., & Or, Y. Y. (2002). Effects of hypoxia and organic enrichment on the coastal marine environment. *Marine Ecology Progress Series*, *238*, 249–279. Retrieved from http://www.jstor.org/stable/24866351

Green, R. E., Breed, G. E., Dagg, M. J., & Lohrenz, S. E. (2008). Modeling the response of primary production and sedimentation to variable nitrate loading in the Mississippi River plume. *Continental Shelf Research*, *28*(12), 1451–1465. https://doi.org/10.1016/j.csr.2007.02.008

Große, F., Kreus, M., Lenhart, H.-J., Pätsch, J., & Pohlmann, T. (2017). A Novel Modeling Approach to Quantify the Influence of Nitrogen Inputs on the Oxygen Dynamics of the North Sea. *Frontiers in Marine Science*, *4*, 383. https://doi.org/10.3389/fmars.2017.00383

Haidvogel, D. B., Arango, H., Budgell, W. P., Cornuelle, B. D., Curchitser, E., Di Lorenzo, E., et al. (2008). Ocean forecasting in terrain-following coordinates: Formulation and skill assessment of the Regional Ocean Modeling System. *Journal of Computational Physics*, *227*(7), 3595–3624. https://doi.org/10.1016/j.jcp.2007.06.016

Hetland, R. D., & DiMarco, S. F. (2008). How does the character of oxygen demand control the structure of hypoxia on the Texas--Louisiana continental shelf? *Journal of Marine Systems*, *70*(1), 49–62. https://doi.org/10.1016/j.jmarsys.2007.03.002

Hetland, R. D., & DiMarco, S. F. (2012). Skill assessment of a hydrodynamic model of circulation over the Texas--Louisiana continental shelf. *Ocean Modelling*, *43-44*, 64–76. https://doi.org/10.1016/j.ocemod.2011.11.009

Hetland, R. D., & Zhang, X. (2017). Interannual Variation in Stratification over the Texas--Louisiana Continental Shelf and Effects on Seasonal Hypoxia. In J. Dubravko, K. A. Rose, R. D. Hetland, & K. Fennel (Eds.), *Modeling Coastal Hypoxia* (pp. 49–60). Springer. https://doi.org/10.1007/978-3-319-54571-4_3

Huang, W.-J., Cai, W.-J., Wang, Y., Hu, X., Chen, B., Lohrenz, S. E., et al. (2015). The response of inorganic carbon distributions and dynamics to upwelling-favorable winds on the northern Gulf of Mexico during summer. *Continental Shelf Research*, *111*, 211–222. https://doi.org/10.1016/j.csr.2015.08.020

Justić, D., & Wang, L. (2014). Assessing temporal and spatial variability of hypoxia over the inner Louisiana--upper Texas shelf: Application of an unstructured-grid three-

dimensional coupled hydrodynamic-water quality model. *Continental Shelf Research*, *72*, 163–179. https://doi.org/10.1016/j.csr.2013.08.006

Laurent, A., & Fennel, K. (2014). Simulated reduction of hypoxia in the northern Gulf of Mexico due to phosphorus limitation. *Elementa Science of the Anthropocene*, *2*. https://doi.org/10.12952/journal.elementa.000022

Laurent, A., Fennel, K., Hu, J., & Hetland, R. (2012). Simulating the effects of phosphorus limitation in the Mississippi and Atchafalaya River plumes. *Biogeosciences*, *9*(11), 4707–4723. https://doi.org/10.5194/bg-9-4707-2012

Laurent, A., Fennel, K., Wilson, R., Lehrter, J., & Devereux, R. (2016). Parameterization of biogeochemical sediment--water fluxes using in situ measurements and a diagenetic model. *Biogeosciences*, *13*(1), 77–94. https://doi.org/10.5194/bg-13-77-2016

Laurent, A., Fennel, K., Cai, W.-J., Huang, W.-J., Barbero, L., & Wanninkhof, R. (2017). Eutrophication-induced acidification of coastal waters in the northern Gulf of Mexico: Insights into origin and processes from a coupled physical-biogeochemical model. *Geophysical Research Letters*, *44*(2), 946–956. https://doi.org/10.1002/2016GL071881

Laurent, A., Fennel, K., Ko, D. S., & Lehrter, J. (2018). Climate Change Projected to Exacerbate Impacts of Coastal Eutrophication in the Northern Gulf of Mexico. *Journal of Geophysical Research: Oceans*, *123*(5), 3408–3426. https://doi.org/10.1002/2017JC013583

Lehrter, J. C., Ko, D. S., Lowe, L. L., & Penta, B. (2017). Predicted Effects of Climate Change on Northern Gulf of Mexico Hypoxia. In D. Justić, K. A. Rose, R. D. Hetland, & K. Fennel (Eds.), *Modeling Coastal Hypoxia: Numerical Simulations of Patterns, Controls and Effects of Dissolved Oxygen Dynamics* (pp. 173–214). Cham: Springer International Publishing. https://doi.org/10.1007/978-3-319-54571-4_8

Levin, L. A., Ekau, W., Gooday, A. J., Jorissen, F., Middelburg, J. J., Naqvi, S. W. A., et al. (2009). Effects of natural and human-induced hypoxia on coastal benthos. *Biogeosciences*, *6*(10), 2063–2098. https://doi.org/10.5194/bg-6-2063-2009

Lohrenz, S. E., Fahnenstiel, G. L., Redalje, D. G., Lang, G. A., Chen, X., & Dagg, M. J. (1997). Variations in primary production of northern Gulf of Mexico continental shelf waters linked to nutrient inputs from the Mississippi River. *Marine Ecology Progress Series*, 45–54. https://doi.org/10.3354/meps155045

Marta-Almeida, M., Hetland, R. ., & Zhang, X. (2013). Evaluation of model nesting performance on the Texas-Louisiana continental shelf. *Journal of Geophysical Research: Oceans*, *118*(5), 2476–2491. https://doi.org/10.1002/jgrc.20163

McDougall, T. J., & Barker, P. M. (2011). Getting started with TEOS-10 and the Gibbs Seawater (GSW) oceanographic toolbox. *SCOR/IAPSO WG*, *127*, 1–28. Retrieved from http://www.teos-10.org/pubs/gsw/v3_04/pdf/Getting_Started.pdf

Ménesguen, A., & Hoch, T. (1997). Modelling the biogeochemical cycles of elements limiting primary production in the English Channel. I. Role of thermohaline stratification. *Marine Ecology Progress Series*, 173–188. https://doi.org/10.3354/meps146173

Ménesguen, A., & Lacroix, G. (2018). Modelling the marine eutrophication: A review. *Science of The Total Environment*, *636*, 339–354. https://doi.org/10.1016/j.scitotenv.2018.04.183

Ménesguen, A., Cugier, P., & Leblond, I. (2006). A new numerical technique for tracking chemical species in a multi-source, coastal ecosystem, applied to nitrogen causing Ulva blooms in the Bay of Brest (France). *Limnology and Oceanography*, *51*(1(2)), 591–601. https://doi.org/10.4319/lo.2006.51.1_part_2.0591

Mesinger, F., DiMego, G., Kalnay, E., Mitchell, K., Shafran, P. C., Ebisuzaki, W., et al. (2006). North American Regional Reanalysis. *Bulletin of the American Meteorological Society*, *87*(3), 343–360. https://doi.org/10.1175/BAMS-87-3-343

Obenour, D. R., Michalak, A. M., Zhou, Y., & Scavia, D. (2012). Quantifying the Impacts of Stratification and Nutrient Loading on Hypoxia in the Northern Gulf of Mexico. *Environmental Science & Technology*, *46*(10), 5489–5496. https://doi.org/10.1021/es204481a

Obenour, D. R., Scavia, D., Rabalais, N. N., Turner, R. E., & Michalak, A. M. (2013). Retrospective Analysis of Midsummer Hypoxic Area and Volume in the Northern Gulf of Mexico, 1985--2011. *Environmental Science & Technology*, *47*(17), 9808–9815. https://doi.org/10.1021/es400983g

Pauer, J. J., Feist, T. J., Anstead, A. M., DePetro, P. A., Melendez, W., Lehrter, J. C., et al. (2016). A modeling study examining the impact of nutrient boundaries on primary production on the Louisiana continental shelf. *Ecological Modelling*, *328*, 136–147.

https://doi.org/10.1016/j.ecolmodel.2016.02.007

Peyronnin, N. S., Caffey, R. H., Cowan, J. H., Justic, D., Kolker, A. S., Laska, S. B., et al. (2017). Optimizing Sediment Diversion Operations: Working Group Recommendations for Integrating Complex Ecological and Social Landscape Interactions. *Water*, *9*(6). https://doi.org/10.3390/w9060368

Rabalais, N. N., Turner, R. E., Wiseman Jr., W. J., & Boesch, D. F. (1991). A brief summary of hypoxia on the northern Gulf of Mexico continental shelf: 1985--1988. *Special Publications*, *58*(1), 35–47. https://doi.org/10.1144/GSL.SP.1991.058.01.03

Rabalais, N. N., Turner, R. E., Dortch, Q., Justic, D., Bierman, V. J., & Wiseman Jr., W. J. (2002). Nutrient-enhanced productivity in the northern Gulf of Mexico: past, present and future. *Hydrobiologia*, *475*(1), 39–63. https://doi.org/10.1023/A:1020388503274

Radtke, H., Neumann, T., Voss, M., & Fennel, W. (2012). Modeling pathways of riverine nitrogen and phosphorus in the Baltic Sea. *Journal of Geophysical Research: Oceans*, *117*(C9), 1–15. https://doi.org/10.1029/2012JC008119

Rosenberg, R., Hellman, B., & Johansson, B. (1991). Hypoxic tolerance of marine benthic fauna. *Marine Ecology Progress Series*, *79*(1/2), 127–131. Retrieved from http://www.jstor.org/stable/44634792

Rosenheim, B. E., Roe, K. M., Roberts, B. J., Kolker, A. S., Allison, M. A., & Johannesson, K. H. (2013). River discharge influences on particulate organic carbon age structure in the Mississippi/Atchafalaya River System. *Global Biogeochemical Cycles*, *27*(1), 154–166. https://doi.org/10.1002/gbc.20018

Rutherford, K., & Fennel, K. (2018). Diagnosing transit times on the northwestern North Atlantic continental shelf. *Ocean Science*, *14*(5), 1207–1221. https://doi.org/10.5194/os-14-1207-2018

Scavia, D., Rabalais, N. N., Turner, R. E., Justić, D., & Wiseman, W. J. (2003). Predicting the response of Gulf of Mexico hypoxia to variations in Mississippi River nitrogen load. *Limnology and Oceanography*, *48*(3), 951–956. https://doi.org/10.4319/lo.2003.48.3.0951

Scavia, D., Bertani, I., Obenour, D. R., Turner, R. E., Forrest, D. R., & Katin, A. (2017). Ensemble modeling informs hypoxia management in the northern Gulf of Mexico. *Proceedings of the National Academy of Sciences*.

https://doi.org/10.1073/pnas.1705293114

Da Silva, A. M., Young, C. C., & Levitus, S. (1994a). *Atlas of surface marine data 1994, Vol. 3, Anomalies of heat and momentum fluxes* (Vol. 8). Washington, D.C.

Da Silva, A. M., Young, C. C., & Levitus, S. (1994b). *Atlas of surface marine data 1994, Vol. 4, Anomalies of freshwater fluxes* (Vol. 9). Washington, D.C.

Simpson, J. H. (1981). The shelf-sea fronts: implications of their existence and behaviour. *Philosophical Transactions of the Royal Society of London A: Mathematical, Physical and Engineering Sciences*, *302*(1472), 531–546. https://doi.org/10.1098/rsta.1981.0181

Strom, S. L., & Strom, M. W. (1996). Microplankton growth, grazing, and community structure in the northern Gulf of Mexico. *Marine Ecology Progress Series*, *130*, 229–240. https://doi.org/10.3354/meps130229

Sylvan, J. B., Dortch, Q., Nelson, D. M., Maier Brown, A. F., Morrison, W., & Ammerman, J. W. (2006). Phosphorus Limits Phytoplankton Growth on the Louisiana Shelf During the Period of Hypoxia Formation. *Environmental Science & Technology*, *40*(24), 7548–7553. https://doi.org/10.1021/es061417t

Task Force. (2001). *Action Plan 2001 for Reducing, Mitigating, and Controlling Hypoxia in the Northern Gulf of Mexico and Improving Water Quality in the Mississippi River Basin*. Washington, D.C.

Task Force. (2014). *New Goal Framework*. Washington, D.C.

Task Force. (2017). *2017 Report to Congress*. Washington, D.C.

Thyng, K. M., Greene, C. A., Hetland, R. D., Zimmerle, H. M., & DiMarco, S. F. (2016). True Colors of Oceanography: Guidelines for Effective and Accurate Colormap Selection. *Oceanography*, *29*. https://doi.org/10.5670/oceanog.2016.66

Troost, T. A., Blaas, M., & Los, F. J. (2013). The role of atmospheric deposition in the eutrophication of the North Sea: A model analysis. *Journal of Marine Systems*, *125*, 101–112. https://doi.org/10.1016/j.jmarsys.2012.10.005

Vaquer-Sunyer, R., & Duarte, C. M. (2008). Thresholds of hypoxia for marine biodiversity. *Proceedings of the National Academy of Sciences*, *105*(40), 15452–15457. https://doi.org/10.1073/pnas.0803833105

White, E. D., Messina, F., Moss, L., & Meselhe, E. (2018). Salinity and Marine Mammal Dynamics in Barataria Basin: Historic Patterns and Modeled Diversion Scenarios. *Water*, *10*(8), 1–26. https://doi.org/10.3390/w10081015

Wiseman, W. J., Rabalais, N. N., Turner, R. E., Dinnel, S. P., & MacNaughton, A. (1997). Seasonal and interannual variability within the Louisiana coastal current: stratification and hypoxia. *Journal of Marine Systems*, *12*(1), 237–248. https://doi.org/10.1016/S0924-7963(96)00100-5

Yu, L., Fennel, K., & Laurent, A. (2015). A modeling study of physical controls on hypoxia generation in the northern Gulf of Mexico. *Journal of Geophysical Research: Oceans*, *120*(7), 5019–5039. https://doi.org/10.1002/2014JC010634

Yu, L., Fennel, K., Laurent, A., Murrell, M. C., & Lehrter, J. C. (2015). Numerical analysis of the primary processes controlling oxygen dynamics on the Louisiana shelf. *Biogeosciences*, *12*(7), 2063–2076. https://doi.org/10.5194/bg-12-2063-2015

Zhang, W. G., Wilkin, J. L., & Schofield, O. M. E. (2010). Simulation of Water Age and Residence Time in New York Bight. *Journal of Physical Oceanography*, *40*(5), 965–982. https://doi.org/10.1175/2009JPO4249.1

Zhang, X., Hetland, R. D., Marta-Almeida, M., & Dimarco, S. F. (2012). A numerical investigation of the Mississippi and Atchafalaya freshwater transport, filling and flushing times on the Texas-Louisiana Shelf. *Journal of Geophysical Research: Oceans*, *117*(11), C11009. https://doi.org/10.1029/2012JC008108

Table 1: Average TN, NPP and SOC and fractions supported by Mississippi and Atchafalaya N sources in the yellow region shown in Fig. 1a from the control, 20%-reduction and 60%-reduction runs for the summer of 2001. Also shown are hypoxic area (A_H) and source-specific NPP and SOC per unit river load in the region west of the Mississippi River delta. Percentages in parentheses indicate relative change compared to the control run.

	TN (mmol N m^{-3})	NPP (mmol N m^{-2} d^{-1})	SOC (mmol O_2 m^{-2} d^{-1})	A_H (10^3 km^2)	NPP/river load (mol N/mol N)	SOC/river load (mol O_2/mol N)
		June-August 2001			May-August 2001	
			Control			
Mississippi	9.8	5.0	8.0	n.a.	2.5	2.9
Atchafalaya	8.3	4.4	6.7	n.a.	1.7	2.2
total	19.8	10.8	16.9	21.9	n.a.	n.a.
			20% N reduction			
Mississippi	7.6 (-23.1%)	4.6 (-7.8%)	7.4 (-8.1%)	n.a.	2.8 (+13.2%)	3.3 (+14.7%)
Atchafalaya	6.3 (-23.5%)	4.2 (-5.3%)	6.3 (-6.2%)	n.a.	2.0 (+17.9%)	2.6 (+17.9%)
total	15.3 (-22.9%)	10.0 (-6.8%)	15.6 (-7.6%)	20.4 (-6.9%)	n.a.	n.a.
			60% N reduction			
Mississippi	3.0 (-69.9%)	3.0 (-40.8%)	4.7 (-41.8%)	n.a.	3.7 (+50.3%)	4.5 (+55.3%)
Atchafalaya	2.8 (-65.6%)	3.2 (-27.2%)	4.6 (-30.4%)	n.a.	2.9 (+69.1%)	3.7 (+72.2%)
total	6.7 (-65.9%)	7.3 (-32.5%)	11.0 (-34.8%)	11.5 (-47.6%)	n.a.	n.a.

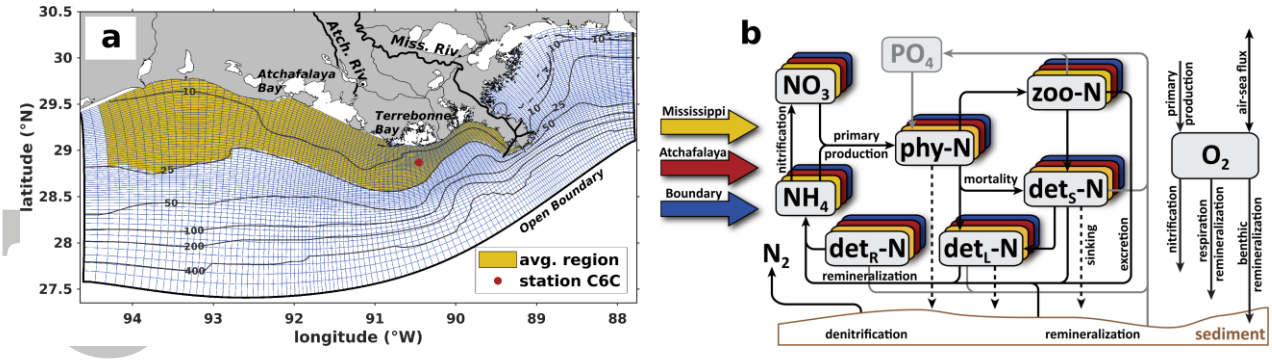

Figure 1: (a) Model grid (blue lines) with time-series station (red dot) and averaging region (yellow area; depth ≤ 25 m). Black lines represent isobaths (in m). (b) Schematic of the model's nitrogen and phosphorus cycles and the processes affecting oxygen. Colored arrows and boxes represent the three different external sources of nitrogen and the additional sets of model tracers tracking their cycling through the model's nitrogen pools.

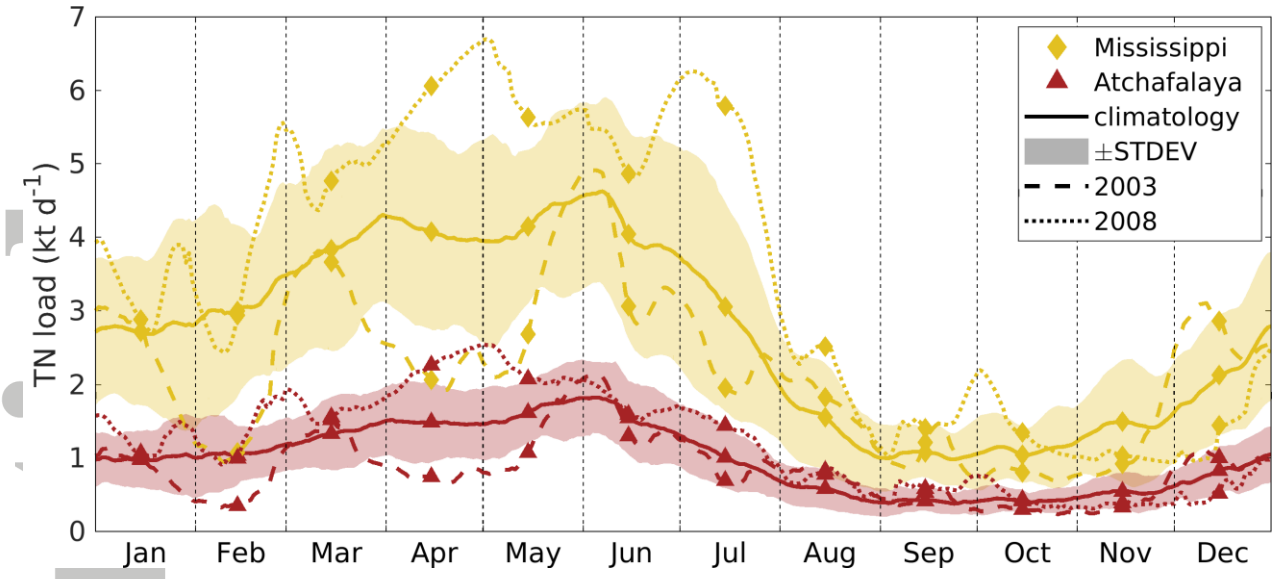

Figure 2: Daily time series of total nitrogen (TN) loads for Mississippi and Atchafalaya Rivers. Solid lines and shaded areas: 2001-2011 climatological average ± one standard deviation (STDEV). Dashed and dotted lines: 2003 and 2008, respectively.

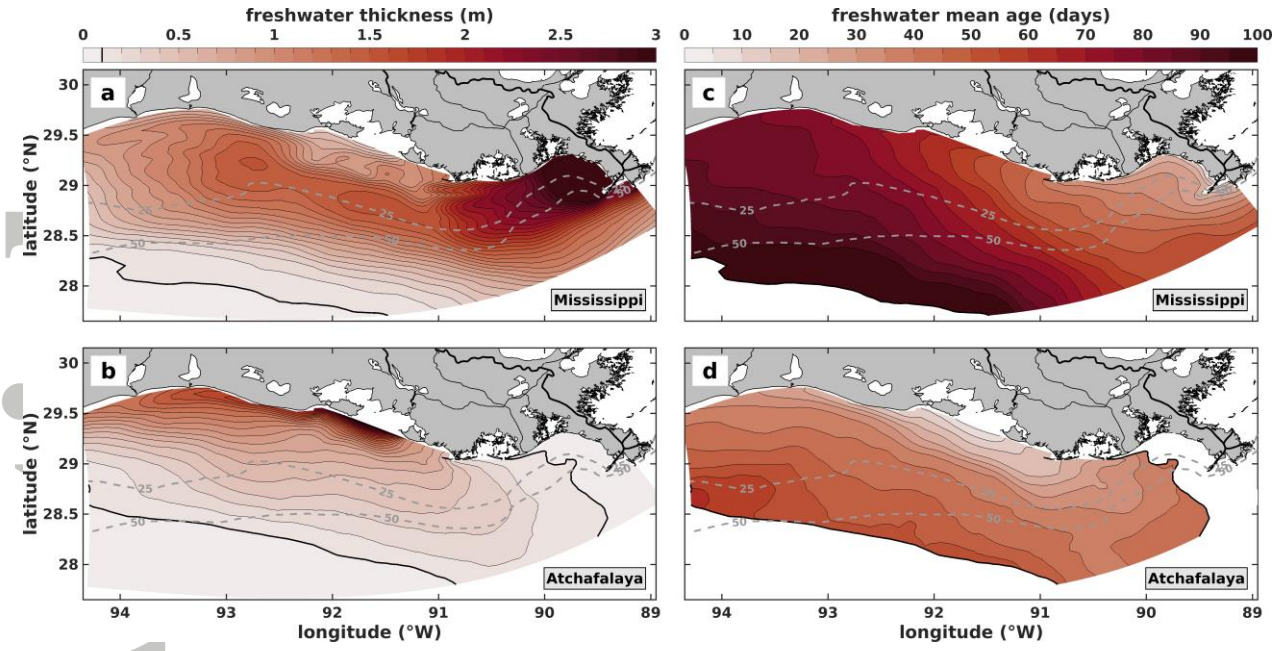

Figure 3: 11-year averaged summer (June-August) (a, b) thickness and (c, d) mean age of (top) Mississippi and (bottom) Atchafalaya freshwater. Mean age is only shown in regions where freshwater thickness is >0.1 m (thick isopleth). Gray dashed lines indicate isobaths (in m).

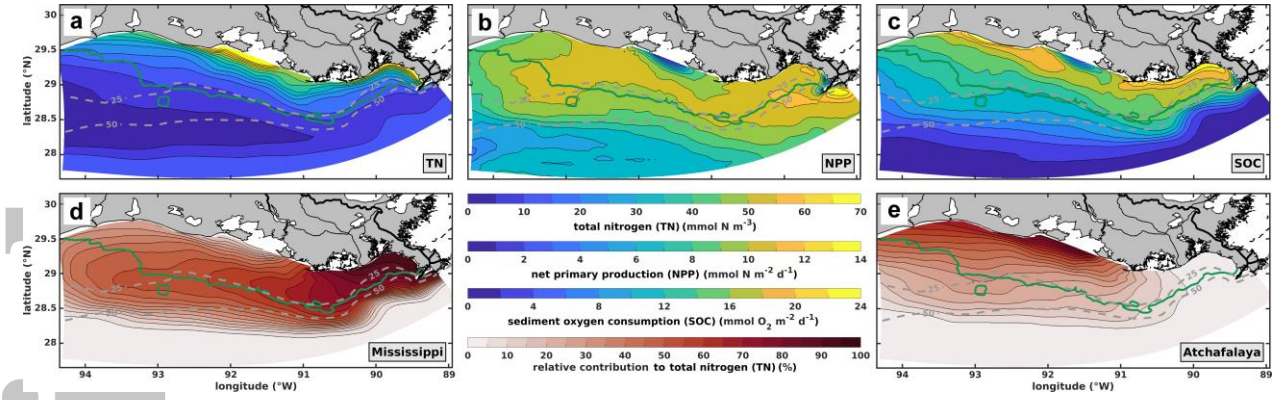

Figure 4: 11-year-averaged summer (June-August), near-surface (0-25m) (a) TN, (b) NPP and (c) SOC, and corresponding relative contributions to TN by (d) Mississippi and (e) Atchafalaya Rivers, respectively. Color scales apply in the order of the panels. Same color scale for (d, e). Solid green line indicates average hypoxic region defined as region with on average at least one day of hypoxia during summer. Gray dashed lines indicate isobaths (in m).

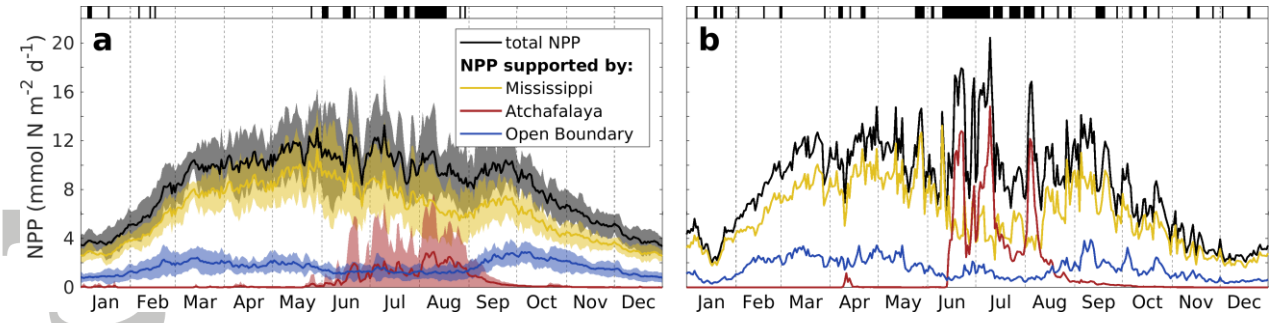

Figure 5: Daily time series of total and source-specific water-column-integrated NPP at station C6C for (a) 2001-2011 (11-year average) and (b) 2009. Markers at the top indicate upwelling-favorable winds derived from spatially averaged, daily zonal wind speed. In (a), shaded areas indicate ± one standard deviation and winds must be upwelling-favorable during at least 5 years to be marked as such. See Fig. 1a for station location and averaging area.

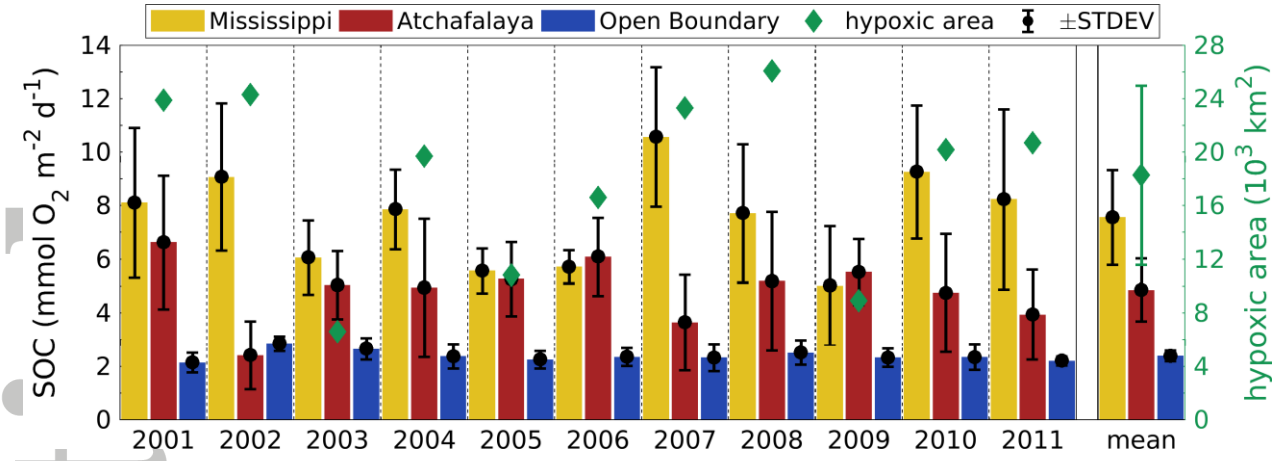

Figure 6: Average daily, source-specific SOC (bars) in region shallower than 25 m (see Fig. 1a) during June-August, and observed hypoxic area (diamonds) from Obenour et al. (2013) for individual years, and averaged over 2001-2011. Error bars indicate standard deviations (STDEV). STDEVs of the 2001-2011 averages are the STDEVs of the averages of the individual years. Values are provided in Table S1.

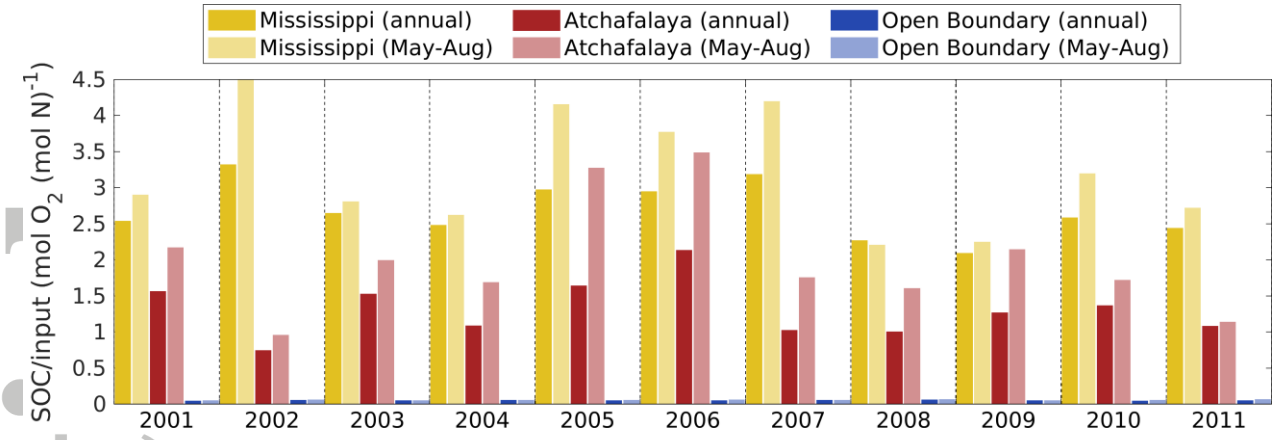

Figure 7: Time series of source-specific SOC per unit of influx in the model domain west of the Mississippi River Delta.

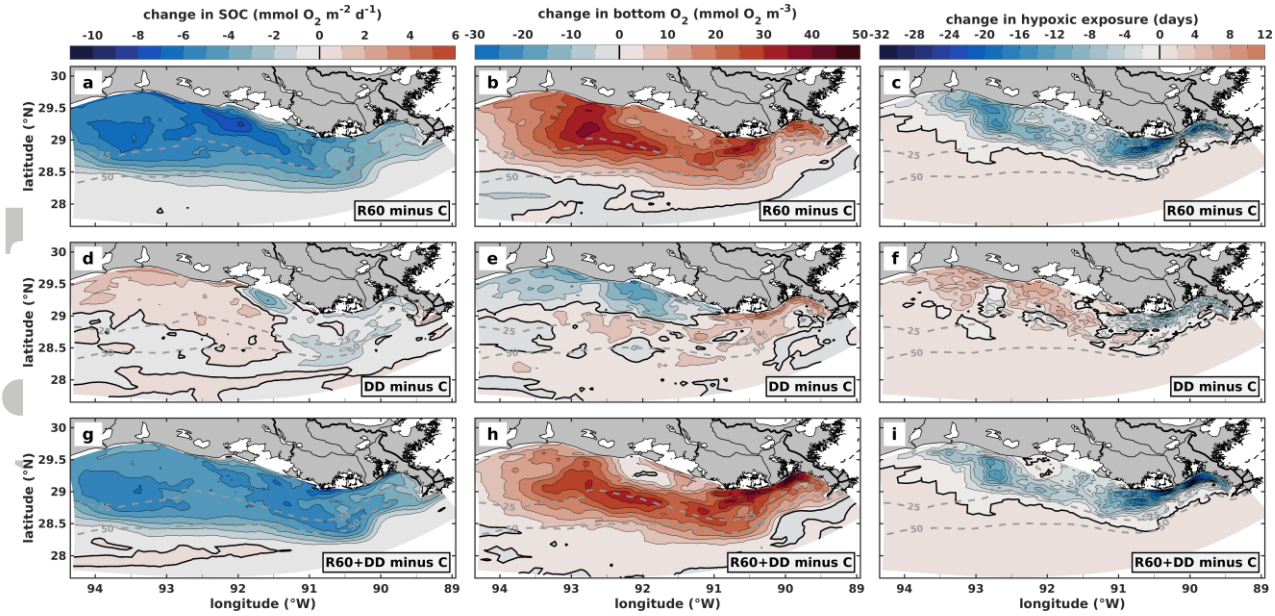

Figure 8: Changes in SOC (left), bottom oxygen concentration (center), and cumulative hypoxic exposure (right) relative to the control simulation (C) for the different model scenarios and averaged over summer (June-August) 2001 to 2011: (a, b, c) 60% N load reduction (R60); (d, e, f) discharge diversion (DD); (g, h, i) combined 60% N load reduction and discharge diversion (R60+DD). Thick isopleths indicate zero change. Gray dashed lines indicate isobaths (in m).